

Entropy-based 3-D Mapping with teams of Cooperative Mobile Robots: a simulation study

Rui Rocha ^(1, 2), Jorge Dias ⁽¹⁾ and Adriano Carvalho ⁽²⁾

⁽¹⁾ Institute of Systems and Robotics, University of Coimbra, PORTUGAL

⁽²⁾ Faculty of Engineering, University of Porto, PORTUGAL

E-mails: {rprocha, jorge}@isr.uc.pt, asc@fe.up.pt

Technical Report, February 9, 2004

Abstract One of the application fields of multi-robot systems is cooperative mapping of an unknown environment. In this article, the problem of mapping an unknown 3-D environment is formulated through a probabilistic model based on information theory. Besides describing how such a map is updated upon new measurements, we use the map to estimate a spatial field of entropy and propose a gradient-based survey strategy which drives the robot to explore map locations having higher entropy (uncertainty). The single robot strategy is extended to a team of such robots which are committed to cooperate by sharing new acquired sensory information. We present an entropy-based measure of information utility which is used by robots to cooperate on building a 3-D map, without overwhelming communication resources with redundant or unnecessary information. The proposed framework is validated through its application to robots equipped with range sensors measuring distance information. Results from a set of simulation experiments on building 3-D coverage maps, with a single robot and with a team of cooperative robots, are presented.

Keywords Cooperative multi-robot systems, 3-D mapping, entropy, information utility.

1 Introduction

Multi-robot systems (MRS) have been widely investigated for the last decade [1, 2, 3]. These systems employ teams of cooperative robots to carry out missions that are either inherently distributed

in time, space, or functionality, and cannot be achieved by a single robot, or where a multi-robot solution is more efficient, cost effective, reliable and robust than a single robot solution. Building a 3-D map of an unknown environment is one of the application fields of MRS. Our work studies two main problems: (i) developing a probabilistic model for 3-D mapping using information theory; and (ii) sharing information efficiently through communication in a team of cooperative mobile robots, driven by the maximization of information utility.

Robotic mapping addresses the problem of acquiring spatial models of physical environments through mobile robots. Some examples of sensors used to build maps are cameras, range finders using sonars, laser or infra-red rays, radars, tactile sensors, etc. As sensors have always limited range, are subject to occlusions and yield measurements with noise, mobile robots have to navigate through the environment and build the map iteratively. Mapping can be classified as [4]: whether they are metric or topological – metric maps capture geometric properties whereas topological maps describe the connectivity of different places; or whether they are world-centric or robot-centric – world-centric maps are represented in a global-coordinate space and robot-centric are represented in measurement space. Some key challenges arises from the nature of measurement noise (sensor modeling problem), high dimensionality of the entities being mapped (representation problem), the correspondence or registration problem (registering measurements on a common coordinate space), dynamically changing environments and defining an efficient survey

strategy to build the map (exploration problem). Robots can be used to build fastidious maps of indoor environments [5, 6, 7, 8], but they are particularly useful on mapping missions of hazardous environments for human beings, such as abandoned underground mines [9, 10], where updated maps are required to prevent future accidents related with inundations or collapses, but where humans access is too risky or even impossible due to difficult access routes; or nuclear facilities [11], where monitoring the state of the sarcophagus interior is required by maintenance procedure, but where humans exposure to radiation must be avoided. Although it is recognized the potential of MRS on such mapping missions, current state-of-the-art of robot mapping is limited to single robot solutions.

Some of the work on robotics for mapping unknown environments has been restricted to 2-D maps and applied mainly to indoor environments. In [12], Moravec et al. developed occupancy grids, a space representation model, which are discretised random fields where the probability of occupancy of each independent cell is maintained. In their seminal work, they built 2-D occupancy grids by using a robot with sonars. In [5], they extended the occupancy grid technique for environment mapping of 3-D grids, using stereo-vision as primary sensor. In [6], a robot equipped with two ultrasonic sensors was used to build a 2-D occupancy grid of an indoor environment, where abnormal sensor measurements were detected and used to adjust a confidence level for each sensor. Vidal et al. [13] used 2-D occupancy grids to represent multi-robot team knowledge about obstacles and evaders within a pursuit-evasion game. Their work focused on developing probabilistic pursuit policies for that specific game theoretical framework. Bourgault et al. [14] also used occupancy grids to address the single robot exploration problem, as a balance of alternative motion actions from the point of view of information gain (in terms of entropy), localization quality and navigation cost. Although they include information gain in their strategy, their formulation is computationally heavy and they were only able to use it off-line, for a limited number of proposed destinations. In [8], the notion of occupancy grid was refined to avoid the binary representation of the cell's occupancy and to model it as a continuous value between 0 and 1. They used 2-D coverage maps to perform indoor exploration tasks

performed by a robot equipped with sonars.

There is some recent work on 3-D mapping with a single robot, focusing mainly on the registration problem. In [15], a mobile mapping system for generating a 3-D model of an indoor environment is presented. The proposed solution is designed to minimize the error propagation due to the registration of measurements relative to the mobile platform in a global reference frame. In [11], a trinocular stereoscopic mapping system for use in post-nuclear accident operations is presented. The idea is constructing a robot equipped with a 3-D mapping system to provide the shelter operators of a nuclear facility with a means of evaluating the state of the sarcophagus interior. The work focus on the processing of surface meshes provided by the vision sensor and data registration in a global reference frame. In [16], a method for building 3-D maps of buried utilities (e.g. gas pipes, power or communications lines, etc.) is developed to detect and extract their features. It is based on sensor fusion of data from an electromagnetic induction sensor and a ground penetrating radar, which are attached to digging equipment used for construction, in order to avoid getting close to already buried utilities. In [7], a method for 3-D digitalization of indoor environments using a laser range finder is presented. The 2-D laser range finder is attached to a servo motor so as it can sweep a 3-D environment through multiple scans. Their map's representation stores detected lines and polygons through Hough transform and the proposed method focus on planning the next scan pose as well as the robot's trajectory. Pose planning is based on three criteria: information gain, robot's accessibility and path length. Whereas we define an entropy-based measure of information gain, their measure is based on a geometric interpretation of the map. Vandapel et al. have been working on developing methods for modeling 3-D environments. In [9], they describe the problem of sensing and generating 3-D models of an underground mine with data gathered from a laser range finder, focusing on the problem of registering 3-D data sets from different views in a common coordinate system. Their registration approach is analogous to assembling a 3-D jigsaw puzzle, with each view being a piece of the puzzle. Thrun et al. [10] addresses the problem of building 3-D volumetric maps of underground mines with laser range finders. They approach mine mapping as a simul-

taneous localization and mapping (SLAM) problem but, due to cyclic structure of mines, SLAM yields difficult correspondence problems. To solve this problem, they use an iterative closest point algorithm, generating 3-D maps by applying scan matching to 3-D measurements after a 2-D mapping of the mine is complete.

As the 3-D mapping research issue involves different difficult problems, it is not possible to cope with all of them simultaneously. Most of the previous research work on 3-D modeling is based on deterministic models without an explicit representation of the map’s uncertainty. There are some exceptions, but whether they are restricted to 2-D maps with a single robot [8] or cannot cope with real-time requirements [14]. Our innovative work within this research topic proposes a 3-D probabilistic representation model and entropy-based efficient survey strategies based on it, both for a single robot and a team of cooperative robots. The strategies drive robots to the most uncertain and less explored map locations. As we have validated our work with experiments on building 3-D coverage maps upon distance measurements, we also deal with probabilistic modeling of range sensors.

Most of the work in MRS has been devoted to the definition of different architectures, mostly behavior-based, that rule the interaction between the behaviors of individual robots [17, 18]. Communication is a central issue of MRS because it determines the possible modes of interaction among robots, as well as the ability of robots to build successfully a world model, which serves as a basis to reason and coherently act towards a global system goal. Communication may appear in three different forms of interaction [1]: (i) *via environment*, using the environment itself as the communication medium (stigmergy); (ii) *via sensing*, when an agent knowingly uses its sensing capabilities to observe and perceive the actions of its teammates; and (iii) *via communication*, using a communication channel to explicitly exchange messages among the agents, thus compensating perception limitations. Arkin [19] demonstrated that sometimes cooperation between robotic agents was possible even in the absence of communication, however this is a weak form of cooperation and it may be very inefficient. Mataric [20] showed that the ability to distinguish other robots from the rest of other objects provides sufficient power to overcome interfer-

ence. Balch et al. [21] made simulation studies of three typical multi-agent tasks, using the three basic communication types referred above, and found that communication improves performance significantly in tasks with little implicit communication and that more complex communication strategies (goal-oriented) offer little benefit over basic communication (state). Within CEBOT framework, Fukuda et al. [22] studied methods that seek to reduce communication requirements, by increasing the awareness level of individual cells. Parker [23] investigated the impact of awareness on a MRS and concluded that it improves performance, regardless of team size. Tambe presented STEAM [24], a general model of teamwork, which includes a heuristic that attempts to follow the most cost-effective method of attaining mutual belief in joint intentions, by managing a tradeoff between communication and team incoherence costs. Stone and Veloso [25] proposed a method for inter-agent communication, which assumes that agents alternate between periods of limited and unlimited communication.

Although previous work on communication structures for MRS has led to some useful conclusions and design guidelines, there is no a principled formalism that can be systematically used to assess information utility and support the efficient use of communication in MRS. Current architectures (e.g. [17, 18]) extensively use explicit communication, not taking care, giving low emphasis, or using no principled heuristics to avoid the communication of redundant information. As communication is always limited, either in resources applied to perceive the world or in bandwidth of a communication channel, using efficiently those resources is crucial to scale up cooperative architectures for teams of many robots, without limiting them to simple reactive and loosely-cooperative systems, with very limited or no awareness. Based on our 3-D probabilistic model of an unknown environment, we propose an entropy-based measure of information utility which is used by robots to cooperate on building a 3-D map, without overwhelming communication resources with redundant or unnecessary information.

This article is organized in the following way. Section 2 presents a probabilistic 3-D volumetric model of an unknown environment and how to update a 3-D map upon new sensory information, based on a Gaussian sensor model. Section 3

presents how entropy can be used to assess map’s uncertainty and introduces a measure of information utility which is used by robots to select and communicate the most useful information. Section 4 is devoted to 3-D mapping with a single robot, being presented a gradient-based survey strategy which drives the robot to the most uncertain map locations. Section 5 extends the survey strategy to a cooperative MRS, proposing a principled method whereby each robot communicates the most useful information. Both sections 4 and 5 present and discuss simulation results of experiments with robots equipped with range sensors and, at the end of section 5, the benefits provided by cooperation are presented. The article ends with conclusions and future work.

2 3-D mapping and sensor representations

An important resource for mapping missions is, of course, a representation model for the map. In this section, we introduce *probabilistic maps* as a means of representing how uncertain is the robots knowledge about the environment. Although the proposed framework can be a general mathematical tool to map any phenomena spatially distributed, as we have validated it through experiments with robots equipped with range sensors providing distance measurements (e.g. stereo-vision system, laser range, sonar, etc.), hereafter we will denote a map as a coverage map, which is a 3-D representation of the environment occupancy with obstacles. For this reason, by the end of this section, we also present a sensor model and how the coverage map can be updated upon new measurements from the robot’s range sensor.

2.1 Volumetric model

One of the most popular space representation models are *occupancy grids*, which are discretised random fields where the probability of occupancy of each independent cell is maintained [12]. They have been extensively used in robotics mainly due to their simplicity and suitability for decision-theoretic approaches. Some recent examples of their application are [14, 13]. The definition of probabilistic map we use was first introduced in

[8], where the notion of *occupancy grid* was refined in order to avoid a strictly binary representation of each cell’s occupancy (free or occupied), through the notions of *coverage* and *coverage map*. The *coverage* of a cell is the portion of the the cell that is covered by obstacles (a value between 0 and 1). A *coverage map* stores for each cell of a given grid a probabilistic belief about its coverage. Our innovation on the use of this space representation is using it for 3-D mapping with a cooperative multi-robot system, in mapping missions not restricted to indoor environments.

Our volumetric model representation model assumes that we define a 3-D discrete grid \mathcal{Y} which divides the robotic team workspace in equally sized voxels (cubes) with edge vsz and volume vsz^3 . The objective of map building is to obtain, for each voxel $l \in \mathcal{Y}$, an estimate as accurate as possible about its coverage c_l . As c_l is a random variable with a domain equal to the the interval $[0, 1]$, we model our knowledge about the voxel’s coverage through a probability density function

$$p(c_l), 0 \leq c_l \leq 1. \quad (1)$$

As we shall see in the next sections, if the sensor model is assumed to be Gaussian, $p(c_l)$ is also Gaussian with parameters μ_l and σ_l . As long as the map is being built, it is expected to decrease the dispersion σ_l . At a given instant time, our 3-D coverage map is

$$p(c) = \bigcup_{l \in \mathcal{Y}} p(c_l), \quad (2)$$

where the coverage of each individual voxel is assumed to be independent from the other voxels’ coverage and thus can be independently updated.

2.2 Sensor model

The probability density function (pdf) $p(c_l | d)$ represents a sensor model whereby measured distances d are converted in estimates of coverage values c_l of a voxel l . We generally don’t know the exact model of the distribution $p(c_l | d)$ but, accordingly with the central limit theorem¹, the normal distribution is a convenient model if we are mainly interested in

¹The central limit theorem states that the mean of any set of variants, with any distribution, having a finite mean and variance, tends to the normal distribution.

obtaining an unbiased estimate of the voxel's mean coverage. As long as new distances are measured, we can say that the distribution is being sampled and that respective samples have a normal distribution with a mean tending to the true mean of voxel's coverage. Thus, our sensor model is a Gaussian

$$p(c_l | d) = N(\mu(d^l, d), \sigma(d), c_l), \quad (3)$$

where d is the new measured distance and d^l the distance of the voxel to the sensor. The mean of the Gaussian is given by

$$\mu(d^l, d) = \begin{cases} 0, & (d^l - d) < -\frac{vsz}{2} \\ \frac{1}{2} + \frac{d^l - d}{vsz}, & |d^l - d| < \frac{vsz}{2} \\ 1, & (d^l - d) > \frac{vsz}{2} \end{cases}. \quad (4)$$

This equation distinguishes three situations: in the first case, the measured distance does not end in the voxel l , with $d^l < d$, and thus it is more likely that the voxel is fully empty (coverage equal to 0); in the second case, the measured distance ends in l and the mean of its coverage is inverse proportional to the amount of the voxel covered by d (a value between 0 and 1); in the third case, the measured distance does not end in the voxel l , with $d^l > d$, and thus it is more likely that the voxel is fully occupied (coverage equal to 1). The standard deviation is given by

$$\sigma(d) = \sigma_{min} + \zeta \cdot d, \quad (5)$$

i.e. it is at least equal to σ_{min} near to the sensor and increases linearly with d . This is a typical behavior of range sensors because accuracy decreases with distance. Accordingly with the definition of coverage pdf given by equation (1), the Gaussian yielded by the sensor model has to be truncated so that the cumulative probability over the coverage domain sums up to one, i.e. $P(0 \leq c_l \leq 1) = 1$. In [8], it is proposed a sensor model based on a mixture of a Gaussian and an uniform distribution, where the latter distribution adds some white noise to ensure a correct normalization when truncating the Gaussian to the range $[0, 1]$. We claim that a better way of normalizing a normal distribution truncated to that interval is to multiply the pdf by a normalization factor

$$\gamma(\mu, \sigma) = \left(\int_0^1 N(\mu, \sigma, x) \cdot dx \right)^{-1}, \quad (6)$$

which preserves the normal distribution instead of summing white noise. As we shall see in the next section, preserving the normal distribution makes the coverage update upon new measures quite simple. Our definition of the Gaussian's mean is also slightly different from [8], for the second case of equation (4). Figure 1 shows an example of the sensor model for a measured distance of $d = 60cm$ and $d^l \in [0, 100]cm$.

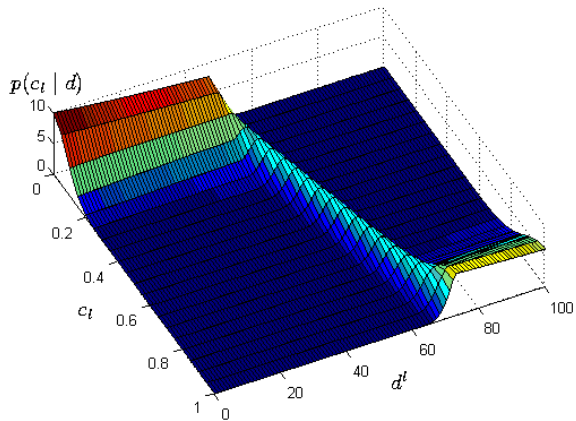


Figure 1: Example of a sensor model: $d = 60cm$, $\sigma_{min} = 0.08$, $\zeta = 0.0005$, $vsz = 25cm$.

2.3 Operations

Consider a given voxel $l \in \mathcal{Y}$ and let

$$\mathcal{D}_n^l = \{d_1^l, \dots, d_n^l\} \quad (7)$$

be the set of all measured distances influencing its coverage. This section specifies how to update the coverage probabilistic belief $p(c_l | D_{n-1}^l)$ and determine the new coverage belief $p(c_l | D_n^l)$ upon a new sensor measurement d_n^l .

The belief about the voxel's coverage can be com-

puted by

$$p(c_l | \mathcal{D}_n^l) = \frac{p(\mathcal{D}_n^l | c_l) \cdot p(c_l)}{p(\mathcal{D}_n^l)} = \quad (8)$$

$$= \beta' \cdot p(c_l) \cdot p(\mathcal{D}_n^l | c_l) = \quad (9)$$

$$= \beta' \cdot p(c_l) \cdot \prod_{i=1}^n p(d_i^l | c_l) = \quad (10)$$

$$= \beta' \cdot p(c_l) \cdot \prod_{i=1}^n \frac{p(c_l | d_i^l) \cdot p(d_i^l)}{p(c_l)} = \quad (11)$$

$$= \beta' \cdot \beta'' \cdot \prod_{i=1}^n p(c_l | d_i^l) = \quad (12)$$

$$= \beta' \cdot \beta'' \cdot p(c_l | d_n^l) \cdot p(c_l | \mathcal{D}_{n-1}^l). \quad (13)$$

Applying Bayes rule, we obtain (8) and (9). Then, if we assume that consecutive distances are independent given the voxel's coverage, we obtain (10). Applying again Bayes rule, we obtain (11). If we assume that $p(d_i^l)$ is constant with i , we finally obtain (12) and (13). The constants β' and β'' are normalization constants ensuring that the left-hand side sums up to one over all c_l . Thus, equation (13) can be used recursively to update the belief $p(c_l | \mathcal{D}_n^l)$ whenever a new influencing distance d_n^l is obtained, by multiplying the current belief $p(c_l | \mathcal{D}_{n-1}^l)$ with the new coverage estimate $p(c_l | d_n^l)$, given the new influencing distance, and applying the normalization factor $\beta' \cdot \beta''$. But this recursive procedure requires the specification of the initial belief $p(c_l | \mathcal{D}_0^l)$, $\mathcal{D}_0^l = \emptyset$.

The initial belief $p(c_l | \mathcal{D}_0^l)$ represents prior knowledge about the voxel's coverage and it is usually chosen to be the less informative, i.e. a pdf with maximum uncertainty. *Entropy* is a general measure for the uncertainty of a belief [26]. Its classical definition applies only to discrete random variables, as it was developed by Shannon as a measure of information for computer networks. However, its definition might be generalized for continuous random variables and, although some care is needed in using it, a number of theorems of entropy apply to both continuous and discrete distributions [27]². The continuous version of entropy is called *differential entropy*. If $f(x)$ is the pdf of a given

²As probability density functions might evaluate to values greater than one, *differential entropy* cannot be taken as an absolute measure of information or uncertainty because it can be negative. However, it provides a relative measure for those properties.

continuous random variable with domain S , it is defined as the expected value of $\log \frac{1}{f(x)}$, which is given by

$$h(f(x)) = - \int_S f(x) \log f(x) dx. \quad (14)$$

The base of the logarithm determines the information unit whereby entropy is measured. We are going to use the base 2 for the logarithm and, in this case, the entropy is measured in bits. Applying the entropy definition to a normal distribution, it can be shown that its differential entropy increases with the logarithm of standard deviation as

$$h(N(\mu, \sigma, x)) = \log_2(\sqrt{2\pi e}) + \log_2(\sigma). \quad (15)$$

It can also be shown that the normal distribution is the maximum entropy pdf given the first two moments. Therefore, equation (15) is a maximum entropy bound for a pdf with variance σ^2 . A convenient initial belief $p(c_l | \mathcal{D}_0^l)$ is thus a normal distribution with $\sigma \rightarrow +\infty$, i.e. an uniform distribution. In practice this means choosing a Gaussian with σ much larger (e.g. ten times greater) than the sensor standard deviation given by equation (5).

At the beginning of the map building process, each voxel has an associated coverage pdf given by a Gaussian with high entropy. As our sensor model (3) is also a Gaussian, when the first measure d_1^l comes, equation (13) involves the multiplication of two Gaussians. If the resultant pdf is also a Gaussian, this process repeats itself whenever new measures are gathered. In fact, it can be easily shown that given two Gaussians $p(c_l | \mathcal{D}_{n-1}^l) = N(\mu_1, \sigma_1)$ and $p(c_l | d_n^l) = N(\mu_2, \sigma_2)$, their product yields a Gaussian multiplied by a constant:

$$p(c_l | \mathcal{D}_{n-1}^l) \cdot p(c_l | d_n^l) = \frac{1}{\beta} \cdot N(\mu, \sigma), \quad (16)$$

$$\mu = \frac{\mu_1 \sigma_2^2 + \mu_2 \sigma_1^2}{\sigma_1^2 + \sigma_2^2}, \quad (17)$$

$$\sigma = \frac{\sigma_1 \sigma_2}{\sqrt{\sigma_1^2 + \sigma_2^2}}, \quad (18)$$

$$\beta = \sqrt{2\pi(\sigma_1^2 + \sigma_2^2)} \exp \left[\frac{(\mu_1 - \mu_2)^2}{2(\sigma_1^2 + \sigma_2^2)} \right]. \quad (19)$$

Comparing equations (13) and (16) we conclude that: updating the coverage belief of a voxel is as simple as computing the parameters of a new

Gaussian through equations (17) and (18); and the normalization constant is $\beta' \cdot \beta'' = \beta$, with β given by equation (19). This simplicity of computation is a consequence of the Gaussian nature of sensor model and our careful choice of an initial coverage belief. Although Gaussians' domain is not restricted to the interval $[0, 1]$, accordingly with equations (4) and (17), we can conclude that $0 \leq \mu_l \leq 1$. In practice, truncating the Gaussian to that interval is not critical to update the coverage belief but, if for some purpose we have to do it, we apply the normalization factor (6)³. Although the mean of the truncated Gaussian is different from μ_l , its mode mode is equal to μ_l and might be taken as a good estimate of the voxel's coverage, because that difference tends to zero provided that $\sigma_l \rightarrow 0$.

Figure 2 shows an example of the aforementioned update procedure. The differential entropy value of depicted pdf's are $H(p(c_l | \mathcal{D}_{n-1}^l)) = -1.911$, $H(p(c_l | d_n^l)) = -1.496$ and $H(p(c_l | \mathcal{D}_n^l)) = -2.233$. While in [8] the coverage belief of a cell

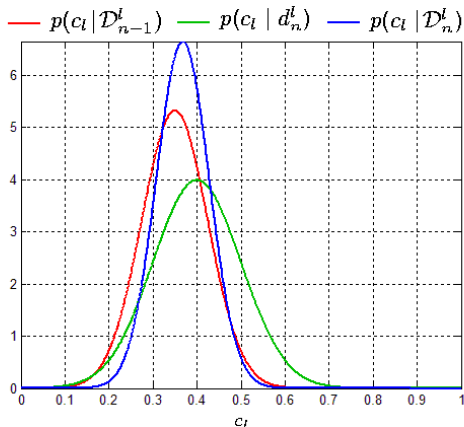


Figure 2: Example of the coverage belief update procedure: $p(c_l | \mathcal{D}_{n-1}^l) = N(0.35, 0.075)$, $p(c_l | d_n^l) = N(0.4, 0.1)$ and $p(c_l | \mathcal{D}_n^l) = N(0.368, 0.06)$.

was represented through histograms with b bins (b is typically more than 10), in our case we represent the voxel's coverage belief as a Gaussian, which is fully characterized by just *two* parameters: μ_l and σ_l . Thus, in the map (2) we have to store only two values for each voxel, which is a much more

³For example, the purpose might be computing a cumulative probability such as $P(0 \leq c_l \leq 0.3)$.

compact representation than a histogram. Moreover, the aforementioned procedure for updating the coverage belief is very simple and we can still build histograms upon the pdf with an arbitrary number of bins.

2.3.1 Influenced voxels by a set of measurements

Whenever the robot's sensor gets a new measurement (distance), we need to determine the set of voxels whose occupancy is influenced by that measurement, and add one more element to the respective set of influencing distances represented through (7). We assume that the output of the robot's range sensor at $t = t_k$, $k \in \mathbb{N}$, is the k -th set of measurements

$$\mathcal{V}^k = \{\vec{v}_1^k, \dots, \vec{v}_{m_k}^k\}, \quad (20)$$

which is a set of m_k 3-D vectors. Each vector $\vec{v}_i^k \in \mathbb{R}^3$ connects the robot's sensor to a 3-D point where an obstacle has been detected. The magnitude of the vectors belonging to the set \mathcal{V}^k is the set

$$\mathcal{D}^k = \{d_1^k, \dots, d_{m_k}^k\} = \{\|\vec{v}_1^k\|, \dots, \|\vec{v}_{m_k}^k\|\}, \quad (21)$$

containing distances between the robot's sensor and the set of points where obstacles have been detected. Each distance d_i^k is used to update the coverage's belief of the set of voxels \mathcal{C}_i^k ; this set contains all the voxels which are traversed by a projective ray collinear with the respective vector \vec{v}_i^k and with origin at sensor's position. The set \mathcal{C}_i^k can be easily determined by sampling that projective ray, so that at least one sample per traversed voxel is gathered in a set of s 3-D points $\mathcal{P} = \{p_1, \dots, p_s\}$. To guarantee this minimum sampling, the projective ray is divided into segments with maximum length equal to the voxel's edge vsz , where the coordinates of each sampling point are given by

$$p_j = pos^k + (j - 1) \cdot vsz \cdot \frac{\vec{v}_i^k}{d_i^k}, \quad 1 \leq j \leq s, \quad (22)$$

being s the sample size and $pos^k \in \mathbb{R}^3$ the sensor's position at $t = t_k$ ⁴. Let $voxel : \mathbb{R}^3 \rightarrow \mathcal{Y}$ be a

⁴In this paper, we does not address the robot's localization issue. It is assumed that the robot can localize itself (its sensor) through some accurate localization scheme and, thus, measurements are automatically well registered in a global coordinates frame.

function that determines what grid's voxel a given point belongs to. We can determine \mathcal{C}_i^k by computing this function to all points in the set \mathcal{P} :

$$\mathcal{C}_i^k = \bigcup_{j=1}^s \text{voxel}(p_j). \quad (23)$$

The set of all voxels influenced by the set of measurements (20) is

$$\mathcal{C}^k = \bigcup_{i=1}^m \mathcal{C}_i^k. \quad (24)$$

The algorithm for updating the map upon the set of measurements (20) might be written in pseudo-code as:

```

for  $i = 1 \dots m_k$ 
  forall  $l \in \mathcal{C}_i^k$ 
     $n \leftarrow n + 1$ 
     $\mathcal{D}_n^l \leftarrow \mathcal{D}_{n-1}^l \cup \{d_i^k\}$ 
    Update  $p(c_l | \mathcal{D}_{n-1}^l)$  upon  $p(c_l | d_i^k)$ 
    and obtain  $p(c_l | \mathcal{D}_n^l)$ 
  end_forall
end_for.

```

3 Entropy and information utility

Whenever a robot gets a new set of measurements as (20), we can say that this event has an associated information utility, which can be measured in terms of a decrease of the map's entropy. Let $H(t_k)$ be the map's entropy at $t = t_k$, which can be explicitly computed as

$$H(t_k) = \sum_{l \in \mathcal{Y}} h(p^k(c_l)), \quad (25)$$

where $p^k(c_l)$ denotes the coverage pdf of voxel l after updating the map with the set (20) and $h(p^k(c_l))$ its differential entropy computed through equation (14). The map's entropy is a measure of the map's uncertainty and its decrease within a period of time is a measure of the information utility of the measurements gathered within the same period of time, in terms of their utility on improving the map's accuracy.

Consider again the sets (20) and (24), representing a set of measurements and the respective set of influenced voxels. Each measurement $\vec{v}_i^k \in \mathcal{V}^k$ influences the coverage of the set of voxels $\mathcal{C}_i^k \subseteq \mathcal{C}^k$ and thus it has also an associated information utility. Let $l \in \mathcal{C}_i^k$ be a voxel whose coverage is influenced by the measure \vec{v}_i^k ; for the same voxel, let also $p(c_l)$ and $p'(c_l)$ be the coverage belief, respectively, before and after the new measurement is integrated. The information utility associated with that measurement is

$$I_i^k = \sum_{l \in \mathcal{C}_i^k} h(p(c_l)) - h(p'(c_l)), \quad (26)$$

which is the respective decrease of coverage entropy. For example, the information utility of the measurement depicted in figure 2 is 0.322. If both coverage beliefs $p(c_l)$ and $p'(c_l)$ are Gaussians, having standard deviations σ_l and σ'_l respectively, accordingly with (15), the information utility associated with the measurement might be computed as

$$I_i^k = \sum_{l \in \mathcal{C}_i^k} \log_2 \left(\frac{\sigma_l}{\sigma'_l} \right). \quad (27)$$

The set of information utilities of measurements in the set (20) is

$$\mathcal{I}^k = \{I_1^k, \dots, I_m^k\} \quad (28)$$

and

$$I^k = \sum_{i=1}^m I_i^k = H(t_{k-1}) - H(t_k) \quad (29)$$

measures the total decrease of the map's entropy due to measurements gathered at $t = t_k$. Equation (25) is a time-consuming computation if it is used at each time step, whenever a new set of measurements is gathered. But, as equation (29) suggests, the map entropy can be recursively updated as $H(t_k) = H(t_{k-1}) - I^k$, which is a much more efficient computation method because it is only computed the entropy of the voxels $l \in \mathcal{C}^k$, whose coverage has just been influenced by the set of measurements \mathcal{V}^k . Thus, equation (25) is only used to compute the maps's initial entropy $H(0)$.

4 3-D maps with a single robot

Accordingly with equation (2), our 3-D map is a set of probability density functions, one for each voxel belonging to the 3-D discrete grid \mathcal{Y} which divides the workspace being mapped. For each voxel $l \in \mathcal{Y}$, the map stores a coverage probability density function $p(c_l)$ which, accordingly with our sensor model, is always Gaussian and thus can be represented through the mean μ_l and the standard deviation σ_l . This section describes how a single robot can be controlled on using such a 3-D map to gather new measurements from regions with higher uncertainty (entropy), and thus to reduce the map's entropy (25) as fast as possible.

Let $coord : \mathcal{Y} \rightarrow \mathbb{R}^3$ be a function that computes the 3-D coordinates $[x_l, y_l, z_l]^T$ of the central point of a voxel $l \in \mathcal{Y}$. The 3-D grid \mathcal{Y} discretises the 3-D space \mathbb{R}^3 at discrete points $coord(l)$, $l \in \mathcal{Y}$, equally spaced by vsz (voxel size). The 3-D map enables us to associate with each of these points a differential entropy $h(l) = h(p(c_l))$ given by equation (14), therefore we might say that a continuous differential entropy field $h : \mathbb{R}^3 \rightarrow \mathbb{R}$ is sampled along the voxels' centers belonging to the grid \mathcal{Y} . The survey strategy we propose claims that the robot's sensor should be directed to regions having higher magnitudes of entropy gradient $\vec{\nabla}h$ and low expected coverage (regions more likely unoccupied), in the neighborhood of the robot. Let assume that each edge of any voxel $l \in \mathcal{Y}$ is aligned with one of the axes (xx, yy or zz) of the global coordinates frame $\{W\}$, and let l_{\ominus} denote the contiguous voxel to l in the negative direction of axis Θ . A reasonable approximation to the entropy gradient at the center of a voxel l is

$$\vec{\nabla}h(l) \approx \frac{1}{vsz} \begin{bmatrix} h(l) - h(l_{x-}) \\ h(l) - h(l_{y-}) \\ h(l) - h(l_{z-}) \end{bmatrix}. \quad (30)$$

Let denote the vector connecting the point $P \in \mathbb{R}^3$ to the center of voxel l as

$$\vec{\tau}(P, l) = \overrightarrow{(coord(l) - P)}. \quad (31)$$

Let $pos \in \mathbb{R}^3$ be the robot's position and $\eta(pos, \xi)$ be the set of voxels at a distance $\xi > 0$ from the current robot's position pos , i.e.

$$\forall l \in \eta(pos, \xi) \subseteq \mathcal{Y}, \quad \|\vec{\tau}(pos, l)\| \leq \xi. \quad (32)$$

Accordingly to the survey strategy we propose, given a neighborhood around the current robot's voxel with radius ξ and the expected coverage $E(p(c_l)) = \mu_l$, the robot is directed to the voxel

$$l_{next} = \operatorname{argmax}_{l \in \eta(pos, \xi)} \left(\|\vec{\nabla}h(l)\| \cdot [1 - E(p(c_l))] \right) \quad (33)$$

with a gaze on arrival defined by the unitary vector

$$\hat{p}_{next} = \frac{\vec{\nabla}h(l_{next})}{\|\vec{\nabla}h(l_{next})\|}, \quad \vec{\nabla}h(l_{next}) \neq \vec{0}. \quad (34)$$

If $\vec{\nabla}h(l_{next}) = \vec{0}$, the gradient-based criteria is not conclusive and the robot should wander until that condition is not verified.

4.1 Coping with robot's kinematic restrictions

Equations (33) and (34) do not cope with robot's kinematic restrictions, assuming that it is able to move freely in the 3-D space. For example, this is suitable for an unmanned aerial vehicle (UAV) but it isn't viable for a ground mobile robot. In order to avoid this assumption, we extend the survey strategy so that new velocity directions near to the robot's motion plane are preferable.

Let $pose = (pos, orient)$ be the current robot's pose, being comprised of three absolute position (translation) coordinates pos and three rotation angles $orient = \{\theta, \phi, \psi\}$, measured in the clockwise direction and representing the robot's attitude. Given a robot's coordinates frame $\{R^{tr}\}$, equal to the global (absolute) coordinates frame $\{W\}$ after translation and rotation, the robot's motion plan Γ is defined by two orthogonal axes: a longitudinal axis $\hat{p}' = [1, 0, 0]^T$, which is the unitary vector along xx axis, and a transverse axis $\hat{q}' = [0, 1, 0]^T$, which is the unitary vector along yy axis; for example, for an UAV, \hat{p} would be the axis between tail and head, and \hat{q} would be the axis connecting the wings. It can be shown that robot's axes can be expressed in a robot's coordinates frame $\{R^t\}$, equal to $\{W\}$ after translation and without rotation, as

$$\hat{p} = [\cos \theta \cdot \cos \phi, -\sin \theta \cdot \cos \phi, \sin \phi]^T, \quad (35)$$

$$\hat{q} = \begin{bmatrix} \cos \theta \cdot \sin \phi \cdot \sin \psi + \sin \theta \cdot \cos \psi \\ -\sin \theta \cdot \sin \phi \cdot \sin \psi + \cos \theta \cdot \cos \psi \\ -\cos \phi \cdot \sin \psi \end{bmatrix}, \quad (36)$$

where the angles have the following definition: angle θ is the robot's yaw angle, being a rotation angle about zz axis; angle ϕ is the robot's pitch angle, being a rotation angle about yy axis; angle ψ is the robot's roll angle, being a rotation angle about xx axis. Note that axis \hat{p} can also be viewed as the robot's gaze direction. Consider again the set of voxels $\eta(pos, \xi)$ satisfying condition (32). Our redefined survey strategy projects any gradient or candidate vector \vec{v} on the robot's motion plan Γ as

$$\text{proj}_{\Gamma} \vec{v} = (\vec{v} \cdot \hat{p})\hat{p} + (\vec{v} \cdot \hat{q})\hat{q}, \quad (37)$$

where (\cdot) denotes the internal product of two vectors. Equations (33) and (34) are thus rewritten as

$$l_{next} = \underset{l \in \eta(pos, \xi)}{\text{argmax}} \left(\rho(pos, l) \cdot \left\| \text{proj}_{\Gamma} \vec{\nabla} h(l) \right\| \cdot [1 - E(p(c_l))] \right) \quad (38)$$

and

$$\hat{p}_{next} = \frac{\text{proj}_{\Gamma} \vec{\nabla} h(l)}{\left\| \text{proj}_{\Gamma} \vec{\nabla} h(l) \right\|}, \quad \text{proj}_{\Gamma} \vec{\nabla} h(l) \neq \vec{0}, \quad (39)$$

where

$$\rho(pos, l) = \begin{cases} \frac{\left\| \text{proj}_{\Gamma} \vec{\tau}(pos, l) \right\|}{\left\| \vec{\tau}(pos, l) \right\|}, & pos \neq coord(l) \\ 1, & \text{otherwise} \end{cases} \quad (40)$$

weights the reachability of a voxel with a value between 0 and 1. For instance, if $\vec{\tau}(pos, l) \perp \Gamma$, the voxel is considered absolutely unreachable and $\rho(pos, l) = 0$.

4.2 Results and discussion

The proposed survey strategy was used to undertake simulation experiments on 3-D mapping with mobile robots. With that purpose, a simulation environment for a 3-D mapping mission was built in MATLAB. The main parameters of the simulator and their respective values are presented in table 1. When measuring with the range sensor, it was assumed that it was able to measure distances within a neighborhood $\{\Delta\theta, \Delta\phi\}$ of the current sensor's orientation $\{\theta, \phi\}$, given by (35). The sensor yield measurements for angles $\{\theta', \phi'\}$ within that neighborhood, through an angular sampling step equal to $pi/90$ rad.

Table 1: Main parameters of the 3-D mapping simulator.

Parameters	Values
Workspace	
Length x Width x Height	10 m x 10 m x 4 m
Voxel size (<i>vsz</i>)	0.25 m
Mobile Robots	
Velocity (maximum)	0.25 m.s ⁻¹
Acceleration (linear)	0.25 m.s ⁻²
Local search radius for navigation (ξ)	0.5 m
Range Sensor	
σ_{min}	0.08
ζ	0.006
Coverage, $\{\Delta\theta, \Delta\phi\}$	$(\pi/6, \pi/12)$ rad
Angular sampling step	$pi/90$ rad

In this section, we present and discuss results obtained with the simulator for a single robot. Each simulated 3-D mapping mission was carried out until the map's entropy, computed through (25), was reduced below a given predefined threshold H_{th} . This stopping criteria has an important associated performance measure for the 3-D mapping mission, which is the instant time $t_{mission} = t_{k_{max}}$ when it is achieved. This instant time verifies the proposition

$$H(t_{mission}) = H(t_{k_{max}}) \leq H_{th} \wedge \forall_{k < k_{max}}, H(t_k) > H_{th}, \quad (41)$$

which states that the k_{max} -th set of measurements is the first one for which the map's entropy is reduced below the threshold. In this study, we have used an initial map where every voxels $l \in \mathcal{Y}$ have an initial Gaussian $p(c_l | \mathcal{D}_0^l)$ with $\sigma_l = 30.0$ which, accordingly with (15) and the workspace parameters in table 1, corresponds to an initial map's entropy $H(0) = 1.987 \cdot 10^5$. The stopping criteria we have used assumed a threshold $H_{th} = -8.6068 \cdot 10^4$, which corresponds, for example, to a final map having Gaussians with $\sigma_l = 0.03$ for the coverage belief of every voxels $l \in \mathcal{Y}$.

The 3-D mapping mission was simulated for a single robot over 10 trials. For each trial, a different starting pose for the robot was chosen. On average, the robot needed $t_{mission} = 2142$ s to accomplish the mission and gathered a total of $k_{max} = 1211$ sets of measurements, with an average size of $\overline{m_k} = 128$ measurements, which yielded a total of 155136 measurements.

Figure 3 shows the graph of the map's entropy $H(t)$ along one of the simulation trials. As the reduction of the map's entropy means information

gain, the symmetric of the derivative of $H(t)$ measures information gain. Therefore, the graph shows that measurements obtained by the beginning of the mission are the most informative (useful) and that measurements' utility decreases as long as the mission is being executed. This agrees with our intuitive expectation that the utility of a measurement decreases as long as knowledge about the environment increases, or as long as uncertainty (entropy) decreases. And this happens because prior knowledge obtained before a given measurement is consequence of the integration of a set of previous measurements and, as long as the size of this set increases, the contribution for that knowledge of an individual (new) measurement is less significant. The curve also shows that a decrease of the threshold H_{th} has a strong impact in $t_{mission}$. Dashed lines in figure 3 show an example where the decrease of map's entropy until $H(t) = H_{th} = -8.6068 \cdot 10^4$ is divided in two equal steps. The robot needed 254.9 s for accomplishing the first step and 1899.5 s for accomplishing the two steps at the final of the mission, which yields an increase of 7.452 in $t_{mission}$ if we go from the first step to the second step.

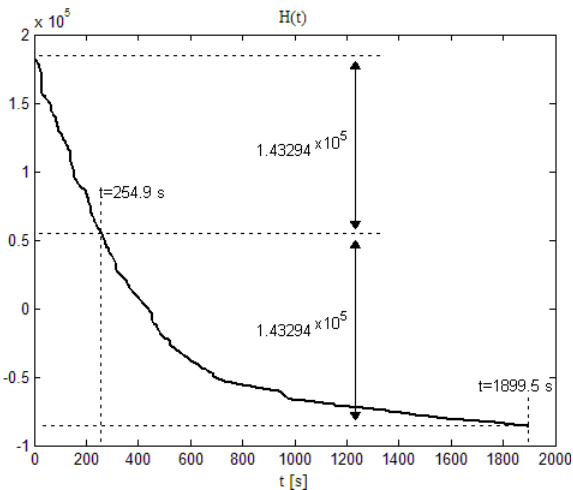


Figure 3: Map's entropy along a 3-D mapping mission with a single robot.

5 3-D maps with a team of cooperative robots

In the previous sections, we have already stated how a single robot can build a 3-D map and how to assess the information utility associated with new sensor measurements. In this section, we describe how a team of such robots, populating the 3-D environment being mapped, can be cooperative on building a 3-D map. Cooperation has three main potential advantages: (i) *efficiency* – taking advantage from the spatial distribution of sensors makes possible to reduce the map's uncertainty more quickly than if a single robot is used; (ii) *reliability and robustness* – with redundancy in robots capabilities, the failure of any particular robot does not necessarily compromise the overall mission success; (iii) *specialization* – robots with different sensory or motion skills may have complementary and specialized features that overcome their individual limitations and increase the team's total utility.

We assume that each robot, besides being able to build and update its own local 3-D map based on information from its own sensors, is also committed to share new acquired sensory information with its teammates through communication. Whenever a given robot gets a set of measurements \mathcal{V}^k , it sends to other robots a list of 3-D coordinates $S^k = (pos^k, \mathcal{U}^k)$. The set

$$\mathcal{U}^k = \{\vec{u}_1^k, \dots, \vec{u}_{mc_k}^k\} \subseteq \mathcal{V}^k \quad (42)$$

is a set of mc_k communicated measurements and pos^k the position of the sensor when those measures were gathered, which is necessary to register those measurements in the local map of other robots⁵. Different communication topologies can be used, depending on the capacity and range of the available communication channel. When possible, the robot acting as information provider should send data to all robots in the team, so that all of them can take advantage of new sensory information; otherwise, the communication is restricted to a team's subset, such as the nearest robots to the information provider.

When a robot receives a list of communicated measurements, it updates its local map as if mea-

⁵As it was already noted, we assume that each robot is able to localize itself accurately and correctly register its sensor measures.

measurements \mathcal{U}^k would have been gathered by its own sensors at the position pos^k (first point in the received list). As communication channels have always limited capacity, when a robot is acting as information provider, it has to limit the amount of communicated data and select the most useful measurements gathered from its own sensors. On doing it, the robot uses equation (26) to assess the information utility \mathcal{I}^k associated with the measurements \mathcal{V}^k and classifies them by utility. Let define $burst$ as being the maximum number of allowable communicated measurements at a given time instant. Let also define I_{min} as being the minimum allowable information utility for a communicated measurement. The set (42) is built in such a way that the proposition

$$\begin{aligned} (mc_k \leq burst \wedge \\ mc_k < burst \Rightarrow \forall_{\vec{v}_z^k \in \mathcal{V}^k \setminus \mathcal{U}^k}, I_z^k < I_{min} \wedge \\ \forall_{\vec{u}_j^k \in \mathcal{U}^k}, I_j^k \geq I_{min} \wedge \forall_{\vec{v}_w^k \in \mathcal{V}^k \setminus \mathcal{U}^k}, I_w^k \leq I_j^k) \quad (43) \end{aligned}$$

is true. In words, the proposition is true (the set of communicated measurements is valid) if the following conditions are met: (a) the size of the set is not greater than $burst$; (b) the size of the set is less than $burst$ only if it includes all measurements in the set \mathcal{V}^k having an information utility not less than I_{min} ; (c) the information utility of communicated measurements is at least I_{min} and all not communicated measurements have lower or equal utility than those which are selected to be communicated.

5.1 Results and discussion

The simulation experiments carried out for the single robot case were extended for teams of cooperative robots with different sizes and for different communication parameters $burst$ and I_{min} . Hereafter, the team size will be denoted as tsz . Our aim was to assess the advantages provided by cooperation and the influence of parameters tsz , $burst$ and I_{min} in the mission execution time $t_{mission}$. Besides using again the parameters already presented in table 1, simulations were carried out with different teams of cooperative robots having combinations of the parameters' values presented in table 2. As our coverage beliefs are always Gaussians, accordingly with (27), if for a given measurement there

Table 2: Sets of values for parameters tsz , $burst$ and I_{min} , used to simulate teams of cooperative mobile robots performing 3-D mapping missions.

Parameter	Set of Values
tsz	{1, 2, 3, 4}
$burst$	{32, 64, 128}
I_{min}	{0.6215, 0.3219, 0.0291}

is only *one* influenced voxel, the values used for I_{min} means a reduction on the standard deviation of the Gaussian for that voxel of 35%, 20% and 2%, respectively. The simulator assumed a broadcast-based communication scheme allowing each robot in the team to communicate measurements to all of its teammates.

5.1.1 Advantages provided by cooperation

Figure 4 presents curves of the map's entropy $H(t)$ of one of the robots in the team, for different team sizes. As it was intuitively expected, increasing the team size accelerates the reduction of the map's entropy and leads to smaller values of $t_{mission}$ because, for a given instant time, the modulus of the derivative of $H(t)$ generally takes higher values as long as tsz is increased. As robots share measurements through communication, each robot is able to integrate in its map a greater number of measurements per time unit and achieves a faster reduction of its maps' entropy. Thus, cooperation has the main benefit of magnifying the sensory capacity of each robot. This fact is demonstrated through the total number of measurements m_T gathered by each robot whose maps' entropy is represented in figure 4. This quantity is computed as

$$m_T = \sum_{k=1}^{k_{max}} (m_k + mc_k) \quad (44)$$

where m_k is the number of measurements yielded by the robot's own sensor at $t = t_k$ and mc_k the number of received measurements through communication by the same robot at the same time instant. The value of m_T is shown near to each curve of figure 4. Observe that, although the four values of m_T are quite similar, those measurements were obtained within time intervals $t_{mission}$ quite different, especially for $1 \leq tsz \leq 3$, $tsz \in \mathbb{N}$. Note

that all of the conclusions aforementioned when discussing the curve for $tsz = 1$ (figure 3) are still applicable to $tsz > 1$.

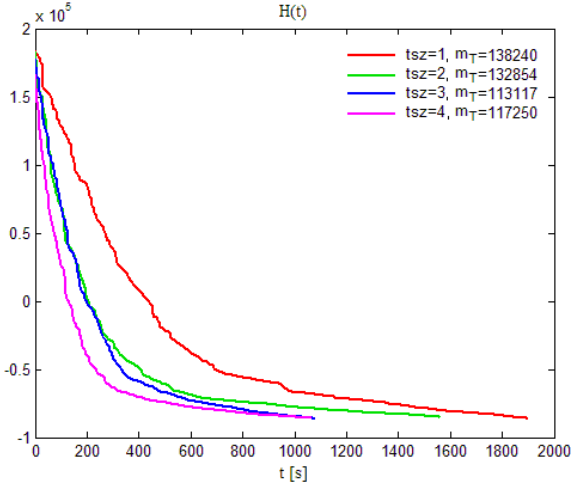


Figure 4: Map's entropy along a 3-D mapping mission for different team sizes. For $tsz > 1$, $burst = 64$ and $I_{min} = 0.3219$.

Figures 5 and 6 show different graphs of $t_{mission}$ as a function of tsz and allows to make a more detailed analysis of the influence of variables tsz , $burst$ and I_{min} on the benefits provided by the cooperation. The curves presented in figure 5 were obtained with different values of $burst$ and $I_{min} = 0.3219$. The curves presented in figure 6 were obtained with different values of I_{min} and $burst = 64$. Both figures confirm the aforementioned conclusion that $t_{mission}$ decreases when tsz increases. However, this performance gain is generally sub-linear, i.e. if tsz increases a times, $a \in \mathbb{N}$, $t_{mission}$ decreases b times, where $b < a$, $b \in \mathbb{R}$. The authors suspect that this performance gain due to a greater team size would be more noticeable, or even super-linear, for a workspace with higher volume, where the benefit of robots' spatial distribution would be more beneficial and interference among robots less prejudicial. But, this conclusion would have to be demonstrated with further simulations. Both figures also show that increasing $burst$ or decreasing I_{min} always leads to higher values of $t_{mission}$ and restricts the effectiveness of cooperation among robots. Both $burst$ and I_{min} restricts the amount of explicit communication among robots, when $burst$

is decreased or when I_{min} is increased (is more selective). In a 3-D mapping mission, there is no communication via environment or via sensing, because robots' actions when performing the mission do not produce changes in the environments which might be sensed by other robots. Thus, as cooperation among robots is based solely on explicit communication, restricting this explicit communication also restricts the extent of cooperation. However, restricting communication is needed for adapting cooperation mechanisms to the communication channel limitations and using it to convey the most useful information. But, figures 5 and 6 do not allow to conclude the way $burst$ and I_{min} restrict communication and cooperation along the mission.

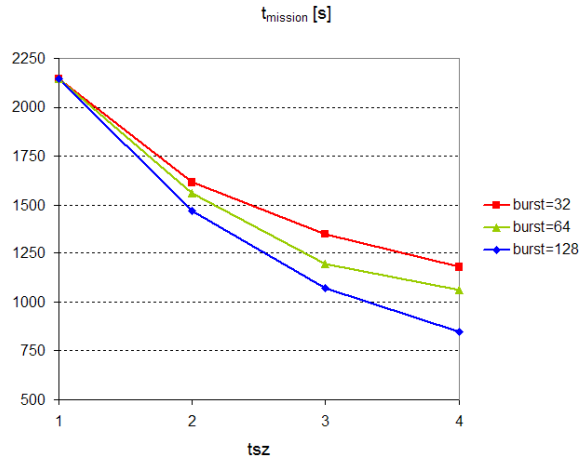


Figure 5: Graphs of $t_{mission}$ as a function of tsz , for different values of $burst$ and $I_{min} = 0.3219$.

Figures 7 and 8 present graphs of the cumulative sum of communicated measurements along the mission. The curves presented in figure 7 were obtained with different values of $burst$ and $I_{min} = 0.3219$. They show that their derivative is nearly the same by the end of the mission and as high as $burst$ at the beginning of the mission. Thus, the parameter $burst$ only restricts communication at the beginning of the mission. This is understandable as the measurements' utility is typically high and greater than I_{min} at the beginning of the mission. The curves presented in figure 8 were obtained with different values of I_{min} and $burst = 64$. As $burst$ is common to the three curves, they show equal derivative for $t = 0$. As long as the mission is exe-

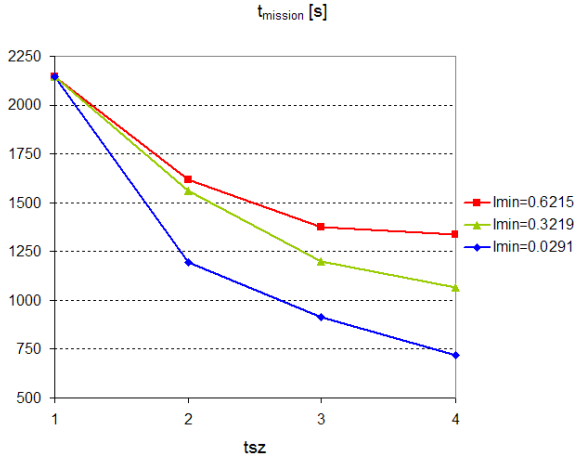


Figure 6: Graphs of $t_{mission}$ as a function of tsz , for different values of I_{min} and $burst = 64$.

cuted, the derivative decreases to an extent which depends on the selectivity of I_{min} , i.e. higher selectivity leads to a smaller derivative by the end of the mission. Thus, the communication limitation due to I_{min} increases with t . Note, for instance, that $I_{min} = 0.0291$ is so small that it does not restrict communication and the curve's derivative is nearly constant along the mission.

These results, about the way $burst$ and I_{min} restrict communication, yield some guidelines for developing communication schemes aiming at fostering cooperation. While the parameter $burst$ is imposed by the communication channel capacity, the parameter I_{min} has to be tuned in an intelligent way, whereby its selective power is beneficial for the performance of the cooperative robotic team. It precludes a robot to communicate measurements with small utility, when other robots might have measurements with much higher utility; this situation is more likely to occur by the beginning of the mission. As long as the 3-D mapping mission is executed and measurements provided by sensors progressively take smaller values, I_{min} becomes more and more restrictive and might lead to a poor utilization of the available communication bandwidth. This suggests that further investigation should be conducted with the aim of developing a selective scheme whereby I_{min} could be adaptively controlled and reduced along the mission.

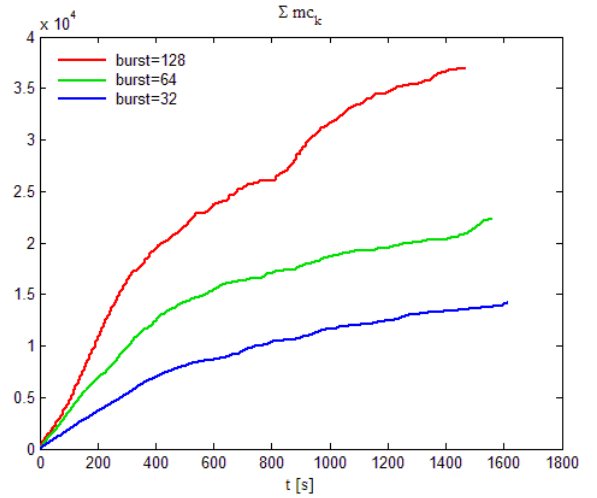


Figure 7: Graphs of the cumulative sum of communicated measurements along a mission, for different values of I_{min} and $burst = 64$.

6 Conclusions

Most of the previous research on building maps of unknown environments has been restricted to deterministic models without an explicit representation of the map's uncertainty. Few authors have proposed a probabilistic approach to the problem, but whether they are restricted to 2-D maps with a single robot or cannot cope with real-time requirements. This article presented innovative work related with developing a probabilistic model for 3-D mapping using information theory to explicitly represent uncertainty, and sharing information efficiently through communication in a team of cooperative mobile robots, driven by the maximization of information utility. We presented a straightforward method to build a 3-D discrete grid, which divides the workspace in equally sized voxels, a sensor model for a range sensor providing distance information, a Bayesian inference procedure to update the coverage belief of each voxel upon new measurements, a gradient-based survey strategy which drives a robot to regions with higher entropy (uncertainty), and an entropy-based measure of information utility which is used by robots to cooperate on building a 3-D map. Simulation results of 3-D mapping experiments with robots equipped with range sensors were presented and discussed,

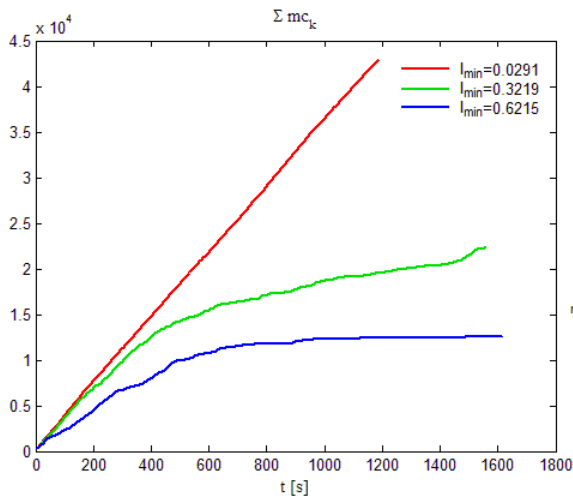


Figure 8: Graphs of the cumulative sum of communicated measurements along a mission, for different values of *burst* and $I_{min} = 0.3219$.

both for a single robot and multi-robot systems with different number of robots. We demonstrated that the proposed framework can be successfully used to perform the 3-D mapping mission. We also showed that a cooperative multi-robot system allows to accomplish the mission in less time and how restricting communication, both in volume and minimum allowed information utility, influences cooperation. Obtained results yielded important guidelines for future development of communication schemes within cooperative multi-robot systems. Future theoretical work will focus on coping with registration of measurements on a common coordinate space, when robots' localization is error-prone. Future experimental will be carried out to validate the proposed models through real mobile robots equipped with active stereo-vision systems.

References

- [1] Y. Cao, A. Fukunaga, and A. Kahng. Cooperative mobile robotics: Antecedents and directions. *Autonomous Robots*, 4:1–23, 1997.
- [2] G. Dudek, M. Jenkin, and E. Milios. A taxonomy of multirobot systems. In T. Balch and L. Parker, editors, *Robot Teams: From Diversity to Polymorphism*. A. K. Peters Ltd., 2002.
- [3] T. Arai, E. Pagello, and L. Parker. Special issue on advances in multirobot systems. *IEEE Trans. on Robotics and Automation*, 18(5):655–864, Oct. 2002.
- [4] S. Thrun. Robotic mapping: a survey. Technical Report CMU-CS-02-111, School of Computer Science, Carnegie Mellon University, Pittsburgh, USA, 2002.
- [5] M. Martin and H. Moravec. Robot evidence grids. Technical Report CMU-RI-TR-96-06, The Robotics Institute, Carnegie Mellon University, Pittsburgh, USA, 1996.
- [6] W. Elmenreich, L. Schneider, and R. Kirner. A robust certainty grid algorithm for robotic vision. In *Proc. of 6th IEEE Int. Conf. on Intelligent Engineering Systems*, Opatija, Croatia, 2001.
- [7] A. Nuchter, H. Surmann, and J. Hertzberg. Planning robot motion for 3d digitalization of indoor environments. In *Proc. of 11th Int. Conf. on Advanced Robotics*, pages 222–227, 2003.
- [8] C. Stachniss and W. Burgard. Mapping and exploration with mobile robots using coverage maps. In *Proc. of IEEE/RSJ International Workshop on Intelligent Robots and Systems (IROS'2003)*, pages 467–472, 2003.
- [9] D. Huber and N. Vandapel. Automatic 3d underground mine mapping. In *Proc of the 4th Int. Conf. on Field and Service Robotics*, July 2003.
- [10] S. Thrun, D. Hhnel, D. Ferguson, M. Montemelo, R. Riebweil, W. Burgard, C. Baker, Z. Omohundro, S. Thayer, and W. Whittaker. A system for volumetric robotic mapping of underground mines. In *Proc. of IEEE International Conference on Robotics and Automation (ICRA'03)*, Taipei, Taiwan, 2003.
- [11] M. Maimone, L. Matthies, J. Osborn, E. Rollins, J. Teza, and S. Thayer. A photo-realistic 3-d mapping system for extreme nuclear environments: Chernobyl. In *Proc. of IEEE/RSJ International Workshop on Intelligent Robots and Systems (IROS'98)*, volume 3, pages 1521–1527, 1998.

- [12] H. Moravec and A. Elfes. High resolution maps from wide angle sonar. In *Proc. of International Conference on Robotics and Automation (ICRA '85)*, Los Angeles, USA, 1985.
- [13] R. Vidal, O. Shakernia, H. Kim, D. Shim, and S. Sastry. Probabilistic pursuit-evasion games: theory, implementation, and experimental evaluation. *IEEE Trans. on Robotics and Automation*, 18(5):662–669, 2002.
- [14] F. Bourgault, A. Makarenko, S. Williams, B. Grocholsky, and H. Durrant-Whyte. Information based adaptive robotic exploration. In *Proc. of IEEE/RSJ International Workshop on Intelligent Robots and Systems (IROS'02)*, pages 540–545, 2002.
- [15] S. El-Hakim, P. Boulanger, F. Blais, and J. Beraldin. A system for indoor 3d mapping and virtual environments. In *Proc. of Videometrics V, SPIE vol. 3174*, pages 21–35, 1997.
- [16] L. Bernold, L. Venkatesan, and S. Suvarna. Multi-sensory approach to 3-d mapping of underground utilities. In *Proc. of Int. Symp. on Automation and Robotics in Construction*, pages 525–530, NIST, Gaithersburg, Maryland, USA, 2002.
- [17] L. Parker. ALLIANCE: An architecture for fault-tolerant multi-robot cooperation. *IEEE Trans. on Robotics and Automation*, 14(2):220–240, 1998.
- [18] M. Matarić and G. Sukhatme. Task-allocation and coordination of multiple robots to planetary exploration. In *Proc. of 10th Int. Conf. on Advanced Robotics*, 2001.
- [19] R. Arkin. Cooperation without communication: Multi-agent schema based robot navigation. *Journal of Robotic Systems*, 9(3):351–364, 1992.
- [20] M. Matarić. Minimizing complexity in controlling a mobile robot population. In *Proc. of IEEE Int. Conf. on Robotics and Automation*, pages 830–835, 1992.
- [21] T. Balch and R. Arkin. Communication in reactive multiagent robotic systems. *Autonomous Robots*, 1(1):27–52, 1994.
- [22] T. Fukuda and K. Sekiyama. Communication reduction with risk estimate for multiple robotic system. In *Proc. of IEEE Int. Conf. on Rob. and Autom.*, pages 2864–2869, 1994.
- [23] L. Parker. The effect of action recognition and robot awareness in cooperative robotic teams. In *Proc. of IEEE/RSJ Int. Workshop on Intell. Robots and Systems*, pages 212–219, 1995.
- [24] M. Tambe. Towards flexible teamwork. *Journal of Artificial Intelligence Research*, 7:83–124, 1997.
- [25] P. Stone and M. Veloso. Task decomposition, dynamic role assignment, and low-bandwidth communication for real-time strategic teamwork. *Artificial Intelligence*, 110(2):241–273, 1999.
- [26] C.E. Shannon. *The Mathematical Theory of Communication*. University of Illinois Press, 1949.
- [27] T. Cover and J. Thomas. *Elements of Information Theory*. Wiley Series in Telecommunications. John Wiley & Sons, 1991.